Orai1 Inhibitors as Potential Treatments for Pulmonary Arterial Hypertension

Bastien Masson, Hélène Le Ribeuz, Jessica Sabourin, Loann Laubry, Emily Woodhouse, Richard Foster, Yann Ruchon, Mary Dutheil, Angèle Boët, Maria-Rosa Ghigna, et al.

Orai1 Inhibitors as Potential Treatments for Pulmonary Arterial Hypertension

Short title: Orai1 Inhibition as a Treatment for PAH

Bastien Masson, PhD[1,2]; Hélène Le Ribeuz, PhD[1,2]; Jessica Sabourin, PhD[3]; Loann Laubry, MSc[1,2]; Emily Woodhouse, PhD[4]; Richard Foster, PhD[4]; Yann Ruchon, MSc[1,2,5]; Mary Dutheil, MSc[1,2,5]; Angèle Boët, MD-PhD[1,2,5]; Maria-Rosa Ghigna, MD-PhD[1,2]; Vincent De Montpreville, MD[6], Olaf Mercier, MD-PhD[7]; David J Beech, PhD[4]; Jean-Pierre Benitah, PhD[3]; Marc A Bailey, PhD, MBChB, MRCS[4]; Marc Humbert,MD-PhD[1,2,8]; David Montani, MD-PhD[1,2,8]; Véronique Capuano, PhD[1,2,5]; and Fabrice Antigny, PhD[1,2]

[1]*Université Paris-Saclay, Faculté de Médecine, Le Kremlin-Bicêtre, France. (B.M, H.L-R, L.R, Y.R, M.D, A.B, M-R.G, M.H, D.M, V.C and F.A)*

[2]*INSERM UMR_S 999 « Hypertension pulmonaire : Physiopathologie et Innovation Thérapeutique », Hôpital Marie Lannelongue, Le Plessis-Robinson, France. (B.M, H.L-R, L.R, Y.R, M.D, A.B, M-R.G, M.H, D.M, V.C and F.A)*

[3]*Inserm, UMR-S 1180, Signalisation et Physiopathologie Cardiovasculaire, Université Paris-Saclay, Châtenay-Malabry, France. (J.S, J-P.B)*

[4]*Leeds Institute of Cardiovascular and Metabolic Medicine, School of Medicine, University of Leeds, United Kingdom. (E.W, R.F, L.C, D.B, M.B)*

[5]*Hôptal Marie Lannelongue, Groupe Hospitalier Paris Saint-Joseph, Le Plessis Robinson, France. (Y.R, M.D, A.B, V.C)*

[6]*Department of Pathology, Groupe Hospitalier-Marie Lannelongue, 92350 Le Plessis-Robinson, France (V.D-M)*

[7]*Service de Chirurgie Thoracique, Vasculaire et Transplantation Cardio-Pulmonaire, Hôpital Marie Lannelongue, Groupe Hospitalier Paris Saint Joseph, Le Plessis Robinson, France. (O.M)*

[8]*Assistance Publique - Hôpitaux de Paris (AP-HP), Service de Pneumologie et Soins Intensifs Respiratoires, Centre de Référence de l'Hypertension Pulmonaire, Hôpital Bicêtre, Le Kremlin-Bicêtre, France. (M.H, D.M)*

Corresponding author: Fabrice Antigny, INSERM UMR_S 999, Hôpital Marie Lannelongue, 133, Avenue de la Résistance, F-92350 Le Plessis Robinson, France.

Tel.: (33) 1 40 94 22 99; E-mail: fabrice.antigny@inserm.fr

ABSTRACT

Rationale: Pulmonary arterial hypertension (PAH) is characterized by progressive distal pulmonary artery (PA) obstruction, leading to right ventricular hypertrophy and failure. Exacerbated intracellular calcium (Ca^{2+}) signaling contributes to abnormalities in PA smooth muscle cells (PASMCs), including aberrant proliferation, apoptosis resistance, exacerbated migration, and arterial contractility. Store-operated Ca^{2+} entry (SOCE) is involved in Ca^{2+} homeostasis in PASMCs, but its properties in PAH are unclear.

Methods: Using a combination of Ca^{2+} imaging, molecular biology, *in-vitro*, *ex-vivo*, and *in-vivo* approaches, we investigated the roles of the Orai1 SOC channel in PA remodeling in PAH and determined the consequences of pharmacological Orai1 inhibition *in vivo* using experimental models of pulmonary hypertension (PH).

Results: SOCE and Orai1 mRNA and protein were increased in human PASMCs (hPASMCs) from patients with PAH (PAH-hPASMCs). We found that MEK1/2, nuclear factor of activated T cells (NFAT), and nuclear factor-kappa B (NFκB) contribute to the upregulation of Orai1 expression in PAH-hPASMCs. Using siRNA and Orai1 inhibitors, we found that Orai1 inhibition reduced SOCE, mitochondrial Ca^{2+} uptake, aberrant proliferation, apoptosis resistance, migration, and excessive calcineurin activity in PAH-hPASMCs. Orai1 inhibitors reduced agonist-evoked constriction in human PAs. In experimental rat models of PH evoked by chronic-hypoxia, monocrotaline, or Sugen/hypoxia, administration of Orai1 inhibitors (BTP2, JPIII, or 5J4) protected against PH.

Conclusions: In human PAH and experimental PH, Orai1 expression and activity are increased. Orai1 inhibition normalizes the PAH-hPASMCs phenotype and attenuates PH in rat models. These results suggest that Orai1 should be considered as a relevant therapeutic target for PAH.

Keywords: proliferation, migration, apoptosis, ATP, mitochondria, calcineurin/NFAT

Non-standard Abbreviations and Acronyms:

SOCE: Store-operated Ca^{2+} entry

PAH: Pulmonary arterial hypertension

PASMCs: Pulmonary arterial smooth muscle cells

PAECs: Pulmonary arterial endothelial cells

NFAT: Nuclear factor of activated T cells

NFκB: Nuclear factor-kappa B

MCT: Monocrotaline

CH: Chronic Hypoxia

Su/Hx: Sugen/Hypoxia

RVSP: Right ventricular systolic pressure

TPR: Total pulmonary resistance

Tg: Thapsigargin

STIM: Stromal Interaction Molecule

CO: Cardiac Output

CSA: Cardiomyocytes cross-section area

Acta1: Actin alpha 1

Actn2: Actinin Alpha 2

Word count (7840/8000)

INTRODUCTION

Pulmonary arterial hypertension (PAH) is a progressive and devastating disease that arises as a consequence of advanced distal pulmonary artery (PA) obstruction (<500 μm in diameter), which leads to high pulmonary vascular resistance (PVR), right ventricular (RV) hypertrophy,

and ultimately right-sided heart failure and death[1]. PAH is defined as a mean PA pressure of >20 mmHg, a PVR of >3 Wood units, and a PA wedge pressure of ≤15 mmHg at rest[2].

The pathophysiology of PAH is multifactorial, involving PA smooth muscle cell (PASMC) dysfunction characterized by hyperproliferation, excessive migration, apoptosis resistance, and vasoconstriction[1]. Current therapeutic strategies for PAH are not curative and focus mainly on controlling endothelial-dependent pulmonary vasomotor tone by targeting three major signaling pathways: the prostacyclin, endothelin-1, and nitric oxide pathways[3]. Despite therapeutic improvements, lung transplantation remains the destination therapy for eligible patients. Thus, identifying novel targets is needed to alleviate pulmonary vascular remodeling in PAH.

Cellular calcium (Ca^{2+}) mishandling is a significant cause of PASMC dysfunction in PAH[4,5]. Although the role of Orai1 in non-excitable cells is well established, the role of Orai1-mediated store-operated Ca^{2+} (SOC) entry (SOCE) in excitable cells, such as PASMCs, remains unclear. Two major SOC components have been identified: the stromal interaction molecule family (STIM1 and STIM2) and the Orai1 Ca^{2+} channel (CRACM1)[6,7]. The contribution of Orai1-mediated SOCE to the proliferation and migration of systemic endothelial and vascular smooth muscle cells (SMCs) has been described[5]. Currently, Orai1 is considered as a potential target for several pathological processes, including asthma and psoriasis[8]. However, the role of Orai1 in pulmonary vascular remodeling remains elusive.

In the present study, we investigated the expression and function of Orai1 in human PASMCs (hPASMCs) isolated from PAH patients (PAH-hPASMCs). We evaluated *in-vivo* the contribution of Orai1 in the development of experimental PH caused by chronic hypoxia (CH), monocrotaline (MCT), and Sugen/Hypoxia (Su/Hx)-exposure in rats.

Overall, we show that Orai1 contributes to pathological phenotype in PAH-hPASMCs. These abnormalities contribute to PA remodeling; therefore, pharmacological inhibition of Orai1 could be a relevant new therapeutic approach to treat PAH.

Materials and methods

Data Availability

The authors declare that all supporting data are available within the article and its online supplementary files.

A detailed description of the Materials and Methods is presented in the Online Data Supplement. Detailed descriptions of all materials and methods used in this study, including chemicals, animals and surgical procedures, pulmonary vascular cell culture, Orai1 knockdown, quantitative reverse transcription-polymerase chain reaction with specific primers (Table I in the online-only Data Supplement), western blot with used antibodies (Table II in the online-only Data Supplement), immunostaining, immunohistochemistry, histological analysis, intracellular Ca^{2+} measurement, Seahorse XF Real-Time ATP Rate Assay, apoptosis measurement, cell proliferation, and cell migration assay, isometric tension measurement echocardiography, Hemodynamic measurements, tissue collection, and statistical analyses are presented in the online-only Data Supplement.

RESULTS

Enhanced Orai1 expression and function in PAH-lung tissue and PAH-hPASMCs.

We first assessed the expression and localization of Orai1 in lung tissues by immunohistochemistry or immunofluorescent staining in paraffin-embedded lung sections from control and PAH patients. We found Orai1 staining in PASMCs and PAECs, with an increased Orai1 staining intensity in remodeled PA from PAH patients (Figure 1A-B). Immunoblots demonstrated higher Orai1 expression in the lungs of PAH patients compared with control subjects (Figure 1C).

The measure of SOCE was performed in control and PAH-hPAECs after Ca^{2+} store-depletion for 10 minutes with 1 µmol/L thapsigargin (Tg) in the absence of external Ca^{2+}. Then SOCE was elicited by adding 2 mmol/L extracellular Ca^{2+} medium. We found that SOCE, SR Ca^{2+}content, and Orai1 protein were unchanged in PAH-hPAECs (Figure 1D-E).

In opposite, the measure of SOCE in PAH-hPASMCs showed an increase in SOCE amplitude with no significant change in SR Ca^{2+} content compared to control (Figure 1F). In association with increased SOCE, Orai1 protein expression was increased in PAH-hPASMCs (Figure 1G), whereas the expression of Orai2 protein was unchanged, and the expression of Orai3 protein was reduced in PAH-hPASMCs (Figure S1).

Because SOCE and Orai1 expression were unchanged in PAH-hPAECs compared to control, we have focused the study on the role of Orai1 in PAH-hPASMCs.

Orai1 knockdown or Orai1 pharmacological inhibition reduces excessive SOCE in PAH-hPASMCs.

The use of siRNA against Orai1 (siOrai1) strongly reduced Orai1 mRNA, Orai1 protein, and SOCE (Figure 2A–C). Moreover, Orai1 blockers, BTP2 (1 µmol/L, also known as YM58483), which is an established and well-known Orai1 channel blocker[9], and JPIII (0.5 µmol/L), a new selective Orai1 blocker[10], reduce SOCE in PAH-hPASMCs and demonstrates the particular importance of Orai1 in SOCE in PAH-hPASMCs (Figure 2D). Similarly, in PAH-hPAECs, siOrai1, BTP2, or JPIII reduced SOCE (Figure S2). These results strongly suggest that the increase in SOCE in PAH-hPASMCs resulted from an upregulation in Orai1 expression.

Since STIM1 is the primary activator of Orai1, we analyzed whether STIM1 could act on Orai1-mediated SOCE in PAH-hPASMCs. Immunofluorescence and immunoblot analysis confirmed that STIM1 was expressed in PASMCs with an unchanged expression in PAH-hPASMCs compared to control-hPASMC (Figure S3A-B). Co-immunoprecipitation showed that Orai1 and STIM1 interacted in PAH-hPASMCs. This interaction was further enhanced after SR Ca^{2+}

depletion with Tg (Figure S3C). In addition, the knockdown of STIM1 reduced SOCE in PAH-hPASMCs (Figure S3D–F). Of note, the expression of STIM2, another isoform of the STIM family that also regulates SOCE[11], was unchanged in the lungs of PAH patients (Figure S4A-B). The knockdown of STIM2 reduced SOCE in PAH-hPASMCs by only 20% without impacting the proliferation of PAH-hPASMCs (Figure S4C-E).

Orai1 inhibition reduced proliferation, migratory capacity, and anti-apoptotic phenotype of PAH-hPASMCs

The contribution of increased Orai1-mediated SOCE in the pathological phenotypes of PAH-hPASMCs was then investigated. *In-vitro* BrdU assay showed that the PAH-hPASMC presented a hyperproliferative phenotype (Figure S5A) as previously described[12]. Inhibition of Orai1 by siRNA or pharmacological inhibition of Orai1 (by BTP2 or JPIII) reduced the proliferation of PAH-hPASMCs by 25-30% (Figure 2E-F). Moreover, PAH-hPASMCs showed enhanced migration compared to control hPASMCs (Figure 2G), and both siOrai1 and pharmacological Orai1 inhibition reduced aberrant migration PAH-hPASMCs (Figure 2H-I and Figure S5B).

In correlation with the reduced proliferation in the siOrai1-treated PAH-hPASMC, we found that siOrai1 increased the expression of the cell cycle inhibitor protein, $P21^{CIP1/Waf1}$ (P21; Figure 2J), which we previously reported being repressed in PAH-hPASMCs[12]. Since PAH-hPASMCs exhibit MAP kinase activation, Akt activation, and reduced Caspase 9 expression, which favors cell proliferation, migration, cell apoptosis, and cell survival pathways[12], we analyzed the activation status of P44/42, caspase 9, Akt, and P38. The knockdown of Orai1 increased the phosphorylation status of P38 (Figure 2K) without any significant changes in total P38 protein level (Figure S5C), in increased caspase 9 cleavage (active form) (Figure 2L), or in pro-caspase 9 level (data not shown). However, knockdown of Orai1 did not affect the expression or

activation (assessed by phosphorylation status) of P42/44 or p308Akt (Figure S5D-E). The transfection agent did not affect Akt1, Cas9, p38 signaling, or P21 expression. (Figure S6).

These data suggest that increased Orai1 expression in PAH-hPASMCs contributes to the pathological phenotype by decreasing P21 expression, P38 signaling, and caspase 9 activity.

An important Ca^{2+}-dependent molecule controlling many cell functions is the serine/threonine phosphatase calcineurin[13]. While the amount of calcineurin protein was unchanged in PAH-hPASMCs compared to control hPASMCs (Figure S5F), a 2-fold increase in calcineurin activity was found in PAH-hPASMCs compared to control hPASMCs. Moreover, Orai1 knockdown or Orai1 pharmacological inhibition (by BTP2 or JPIII) reduced calcineurin activity by 50% (Figure 2M). Thereby, enhanced Orai1 function in PAH-hPASMCs contributes to over-activity of calcineurin, to higher proliferative rate and migratory capacity.

Orai1 channels contributed to pulmonary artery (PA) contraction.

The role of PASMCs is to contract and thereby constrict the PA. The PA from PAH patients is characterized by vasoconstriction[14]. Thus, we assessed the role of Orai1 in human PA tone. BTP2 or JPIII did not affect contraction evoked by increasing doses of KCl (10–90 mmol/L) (Figure 3A-C), while BTP2 or JPIII induced a shift to the right of the dose-response curve for U46619, a thromboxane A2 receptor agonist (0.1–3 μmol/L), indicating that the Orai1 channel contributes to PA constriction induced by thromboxane A2 mimetics (Figure 3B-D).

Orai1-mediated SOCE contributes to mitochondrial Ca^{2+} homeostasis.

As mitochondrial Ca^{2+} homeostasis can modulate cell survival[15], we measured the mitochondrial Ca^{2+} uptake during SOCE using the mitochondrial Ca^{2+} indicator Rhod-2–AM. Mitochondrial Ca^{2+} uptake was increased in PAH-hPASMCs compared to control-hPASMCs (Figure 4A). In PAH-hPASMCs, the siOrai1 reduced mitochondrial Ca^{2+} uptake (Figure 4B) without consequences on mitochondrial membrane potential, mitochondrial shape, and

mitochondrial ATP production (Figure S7). These results suggest that Orai1 could partially enhance the survival of PAH-hPASMCs by modulating mitochondrial Ca^{2+} uptake.

Orai1 knockdown aggravates staurosporine-induced apoptosis in PAH-hPASMCs

To further evaluate the putative role of Orai1 in the apoptosis resistance of PAH-hPASMCs, we exposed cells to staurosporine (apoptosis inducer) at 1 μmol/L for 20 minutes or 50 nmol/L overnight. During 20 minutes of staurosporine exposure, Orai1 knockdown did not influence the apoptotic status of PAH-hPASMCs (Figure S8). In contrast, for longer-term exposure to staurosporine (overnight), the knockdown of Orai1 increased the number of Annexin V-positive PAH-hPASMCs, which suggested more apoptotic cells as well as a concomitant decrease in the number of live PASMCs (Figure 4C-D). An increase in Annexin V-positive cells was also found after BTP2 treatment (Figure 4E-F).

Moreover, the staurosporine overnight exposure of siOrai1-transfected PAH-hPASMCs increased the caspase 9/pro-caspase 9 ratio and the pP38/P38 ratio (Figure 4G-H), while Akt expression/activation and survivin expression were decreased (Figure 4I-K). There was no significantly different between siControl and the transfection agent (Figure S9). These results indicate that low expression of Orai1 makes PAH-hPASMCs more sensitive to apoptosis by overactivation of caspase 9 and P38 and reduced Akt/survivin signaling axis. Therefore, overexpression of Orai1 in PAH-hPASMCs contributes to apoptosis resistance of PAH-hPASMCs, and its knockdown or inhibition of Orai1 counteracts this pathological phenotype.

MEK1/2 signaling, NFAT and NFkB regulate Orai1 expression or function in hPASMCs

As PAH-hPASMCs are characterized by overactivation of MAPK (P42/44, P38) and pro-survival pathways (Akt, calcineurin), we investigated the contribution of these signaling pathways in the increased expression or function of Orai1. We found that the amount of Orai1 protein was reduced in PAH-hPASMCs treated with MEK1/2 inhibitor (UO126), whereas P38 and Akt inhibitors treatment (SB203580 and MEK2206, respectively) had no consequences on

the amount of Orai1 protein (Figure 5A). At the mRNA level, we found that UO126 treatment did not change significantly the Orai1 mRNA expression in PAH-hPASMCs (Figure 5B), suggesting that MEK1/2 regulates Orai1 expression by translational/post-translational regulation. In accordance with the decreased Orai1 expression in UO126-treated cells, SOCE amplitude was reduced following this treatment (Figure S10A).

We also evaluated the contribution of two major transcription factors, NFAT and NFκB, in regulating Orai1 expression. The protein expression of Orai1 and SOCE amplitude were decreased in PAH-hPASMCs, treated with NFAT inhibitor (MCV1) or NFκB inhibitor (PDTC) (Figure 5C, Figure S10B), without any significant changes in Orai1 mRNA level (Figure 5D). These results suggest that the calcineurin/NFAT axis and NF-κB regulate the amount of stable Orai1 protein by a translational/post-translational mechanism.

Since decreased KCNK3 and BMPR2 are a hallmark of different forms of PAH, we used siRNA against BMPR2 or KCNK3 in control-hPASMCs to determine whether KCNK3 or BMPR2 reduced expression acts on the Orai1 expression. After validating our siRNA by RT-qPCR, we found that siKCNK3 had no effect significant consequences on Orai1 mRNA expression but increased Orai1 protein expression (Figure 5E-G), suggesting translational/post-translational control. This appears, at least in part, to be mediated by MEK1/2 and NF-kB pathways since the treatment with PDTC or UO126 reduced the increase of Orai1 protein amount induced by KCNK3 knockdown (Figure 5H). Contrary to KCNK3, the knockdown of BMPR2 in control-hPASMCs did not change significantly the amount of Orai1 protein (Figure 5I-J). This result indicates that the loss of BMPR2 signaling is not related to Orai1 expression in PAH-hPASMCs. Moreover, we did not find a significant change in Orai1 expression in control-hPASMCs exposed to endothelin-1 or PDGF (Figure S10C). These results indicated that increased MEK1/2, NFAT, NFκB activities, and decreased KCNK3 expression could mediate increased Orai1 expression and function by translational/post-translational regulations in PAH.

***In-vivo* pharmacological Orai1 inhibition reduces the development of Chronic-Hypoxia (CH)-induced PH in rats.**

Since Orai1 over-expression/function contributes to aberrant PAH-hPASMCs phenotypes, we next assessed the consequences of *in-vivo* pharmacological inhibition of Orai1 in experimental PH rats models. Like in human lung tissue, immunofluorescent staining showed the expression of Orai1 in PASMCs from normoxic and CH rats with a higher fluorescence intensity in CH lung tissue (Figure 6A). Immunoblot showed an increase in Orai1 protein amount in CH lung tissue (Figure 6B). We then administered BTP2 *in vivo* from week 2 to week 3 to CH rats (Figure 6C). In the CH + BTP2 group, we found an improvement in RV hypertrophy (Fulton's index, Figure 6D) and in RV systolic pressure (RVSP, Figure 6E) compared with the CH + DMSO group. Cardiac output (CO) and heart rate were similar in all experimental groups (Figure 6F and Table S3). Total pulmonary resistance (TPR) was significantly reduced in the CH + BTP2 group compared with the CH + DMSO group (Figure 6G). The BTP2 treatment corrected aberrant pulmonary vascular remodeling induced by CH in rats (Figure 6H–I). While BTP2 treatment reduced the p-P38/P38 ratio in remodeling lungs from CH-rats, no significant change in P42/44, Akt1 activation, or twist1 signaling pathway was observed (Figure S11A-B). Since Orai1 may also contribute to the left ventricular (LV) remodeling[10], we investigated the putative role of Orai1 on RV remodeling. We found unchanged RV mRNA Orai1 levels in CH-rats compared with control rats and similar localization of Orai1 (Figure 6J-K). However, in association with the reduction of RV blood pressure and pulmonary vascular remodeling, we measured a decrease in CH-induced RV fibrosis and a decrease in cardiomyocytes cross-section area (CSA) in CH + BTP2 animals (Figure 6L-M). This RV dysfunction may result from a defect in cardiomyocyte apoptosis since Caspase9 protein expression was reduced in CH + BTP2 animals (Figure S11C) but was unrelated to Akt1 signaling (Figure S11D). Associated with the reduction of RV hypertrophy in CH+BTP2 animals, we found a reduction in mRNA

expression of cardiac hypertrophic markers NPPA (ANP), Acta1 (actin alpha 1), and Actn2 (Actinin Alpha 2) (Figure S11E). Together, these results indicate that pharmacological blockade of Orai1 reduces CH-induced PH in rats.

***In-vivo* pharmacological Orai1 inhibition reduces the development of MCT-induced PH in rats.**

Orai1 immunostaining in lungs from control and MCT rats revealed an expression in PASMCs (Figure 7A). Moreover, Orai1 mRNA and protein expression were increased in isolated PAs from MCT rats compared with control rats (Figure 7B–C). We also found an increase in Orai1 expression in MCT-PASMCs associated with an increased SOCE (Figure 7D-E). The use of BTP2 or JPIII reduced MCT-enhanced SOCE (Figure 7F), confirming that these inhibitors are also effective in inhibiting Orai1 from second rodent species. The *in-vivo* pharmacological inhibition of Orai1 (Figure 7G) improved RV hypertrophy (Figure 7H), RVSP (Figure 7I), CO (Figure 7J), and TPR (Figure 7K) compared to MCT + DMSO group. BTP2 treatment comprehensively corrected aberrant pulmonary vascular remodeling (Figure 7L-M). This remodeling was unrelated to MAPK (p42-44, P38) activation (Figure S12A-B). However, the effect of BTP2 in MCT-induced pulmonary vascular remodeling may result from dysregulation of Akt and twist signaling that were increased and decreased, respectively (Figure S12A-B).

In RV from MCT-PH rats, mRNA Orai1 level was increased and associated with altered localization of Orai1 (more localized at cardiomyocyte junctions, Figure 7N-O), suggesting dysregulation of Orai1 in RV cardiomyocytes from MCT-PH as we previously suspected[16]. Additionally, we found that BTP2 reduces the MCT-induced RV fibrosis and RV cardiomyocytes CSA (Figure 7P). As BTP2 effect in CH rat model, in MCT-induced PH Orai1 inhibition by BTP2 reduced mRNA expression of NPPB, NPPA, Acta1, Actn2, and Caspase 9 protein expression without significant change in Akt expression and activation (Figure 7Q and Figure S12C-E). No significant change in heart rate and stroke volume were observed between

MCT + DMSO and MCT + BTP2 groups (Table S3). These results demonstrate that pharmacological inhibition of Orai1 reduces PH development in rats exposed to MCT.

***In-vivo* pharmacological Orai1 inhibition reduces the development of Sugen/Hypoxia-induced PH in rats**

Finally, in Sugen/Hypoxia (Su/Hx)-induced PH in rats, we also found a benefit in Orai1 inhibition by BTP2 (Figure 8A). In the Su/Hx + BTP2 group, RV hypertrophy (Figure 8B), RVSP (Figure 8C), CO (Figure 8D) and TPR (Figure 8E) were improved compared to Su/Hx + DMSO group. We also found that BTP2 treatment in Su/Hx animals reduced pulmonary vascular remodeling, RV fibrosis, and RV CSA (Figure 8F-I) in association with a reduced mRNA expression of NPPB, NPPA, and Actn2 (Figure S13). No significant change in heart rate and stroke volume were observed between Su/Hx + DMSO and Su/Hx + BTP2 group (Table S3). Therefore, *in-vivo* Orai1 inhibition reduces PH in Su/Hx rats.

To confirm the potential therapeutic benefit of Orai1 inhibition in PH, we administered JPIII to MCT rats. Due to the short *in-vivo* half-life of JPIII[10], we assigned continuous delivery of vehicle (DMSO) or JPIII by osmotic mini-pump from week 1 to week 3 (Figure S14A). In the MCT + JPIII group, RV hypertrophy, RVSP, TPR, pulmonary vascular remodeling, RV fibrosis, and RV cardiomyocytes CSA were reduced (Figure S14B-I). No significant change in heart rate and stroke volume were observed between MCT + DMSO and MCT + JPIII groups (Table S3). We also confirmed the benefit of Orai1 inhibition in MCT-rats by administrating a third Orai1 inhibitor (N-[[(6-Hydroxy-1-naphthalenyl)amino]thioxomethyl]-2-furancarboxamide, herein referred as 5J4).[17] We administered 5J4 from W2 to W3 (Figure S15A). 5J4 treatment attenuated the development of PH (RV blood pressure, RV hypertrophy, pulmonary vascular remodeling, RV fibrosis, RV cardiomyocytes CSA, and no significant change in heart rate (Figure S15B-I, Table S3).

DISCUSSION

Using a combination of Ca^{2+} imaging, molecular biology, *in-vitro*, *ex-vivo*, and *in-vivo* approaches, we found evidence of an essential contribution of the Orai1 Ca^{2+} channel in the development of PAH. First, we found that increased Orai1 expression/function contributes to increased hPASMCs proliferation, migration, apoptosis resistance, and pulmonary vasoconstriction. Second, we showed that Orai1 overactivation highly contributes to increasing calcineurin activity in PAH-hPAMCs. Third, our study uncovered that Orai1 over-expression and over-activity could be partly attributed to MAPKinase signaling pathways, NFAT, and NFkB activity. Fourth, we showed in PAH-hPASMCs that Orai1 over-activity mediated the elevation of mitochondrial Ca^{2+} uptake. Fifth, we highlighted that *in-vivo* pharmacological Orai1 inhibition using three inhibitors (BTP2, JPIII, and 5J4) attenuates the development of PH in three different experimental models. Finally, *in vivo* Orai1 inhibition improves RV fibrosis and hypertrophy in experimental PAH animals.

Orai1 expression and regulation in PASMCs

Several studies have shown the presence of Orai1 in human, mouse, and rat PASMCs, and found that SOCE amplitude is increased in hPASMCs and rat PASMCs after exposure to hypoxia[5]. In this study, we show that Orai1 expression is increased in PAH-hPASMCs and that pharmacological inhibition or knockdown of Orai1 reduces Orai1-induced increase in SOCE amplitude. Also, in proliferative rat aortic SMCs, Orai1 expression is higher than in contractile rat aortic SMCs[18]. Wang et al. demonstrated that hypoxia-inducible factor 1 alpha (HIF1α) upregulated the expression of Orai1 in lung cancer cells[19]. We have previously shown an upregulation of HIF1α in PAH patients[20] and in KCNK3 knockdown condition[20], which may contribute to Orai1 overexpression in PAH-hPASMCs. Moreover, platelet-derived growth factor (PDGF), which is also increased in PAH, enhances Orai1 expression and function in hPASMCs via overactivation of the Akt/mTOR pathway[21]. In PAH-hPASMCs, our

pharmacological approach showed that MEK1/2, NFAT, and NFkB signaling regulate the Orai1 protein expression at the translational/post-translational level unrelated to P38 and Akt signaling. In control-hPASMCs, we discovered that KCNK3 partly controls translational/post-translational Orai1 expression and not PDGF or endothelin-1 signaling. Further studies will be necessary to fully understand the mechanisms responsible for Orai1 overexpression in PAH.

The role of Orai1 in cell proliferation is described in proliferative systemic SMCs[18]. This study shows that Orai1 contributed to the hyper-proliferative phenotype of PAH-hPASMCs. This did not affect the regulation of the pro-oncogenic p42/44 pathway, but it did result from the downregulation of the cell cycle inhibitor, P21.

Role of Orai1 in regulating cell apoptosis

One of the deleterious phenotypes of PAH is the apoptotic resistance of PASMCs. Our study demonstrated that Orai1 knockdown or pharmacological inhibition promotes PAH-hPASMC apoptosis, suggesting that Orai1 overexpression promotes apoptosis resistance. In prostate cancer cells, downregulation of Orai1 protects cells from staurosporine-induced apoptosis[22]. *In-vivo* silencing of Orai1 in mice protects macrophages against apoptosis[23]. Conversely, pharmacological inhibition or silencing of Orai1 in human B lymphoma cell lines leads to an enhancement in apoptosis via activation of the caspase pathway[24]. In the LV pressure overload model, the heart from *orai1*$^{+/-}$ mice had more apoptotic cells than wild-type mice[25]. Here, we found that Orai1 knockdown in PAH-hPASMCs induced overactivation of the caspase 9 cascade and P38 signaling pathway, both known to promote or facilitate apoptosis in several cell types[26]. In addition to the caspase cascade, P38 plays a crucial role in balancing cell survival and death[27].

Moreover, the P38 signaling cascade could regulate apoptosis by regulating the caspase cascade[26]. In contrast to P38, we found that Akt activation was unchanged in siOrai1 PAH-hPASMCs without staurosporine treatment. Nevertheless, in staurosporine-induced apoptosis,

knockdown of Orai1 increased P38 activation and reduced Akt signaling, resulting in a decrease in survivin expression.

Role of Orai1 in regulating calcineurin activity

One of the main proteins regulating intracellular Ca^{2+} concentration is calcineurin, a protein phosphatase that activates the transcriptional factor NFAT. The calcineurin/NFAT axis plays a crucial role in many cellular functions, including proliferation, migration, and apoptosis[28]. A loss-of-function mutation in Orai1 prevented calcineurin/NFAT activation in T cells[30]. Recently, Kar et al. demonstrated that the N-terminus of Orai1 couples to AKAP79 to drive calcineurin/NFAT activation by Ca^{2+} entry nanodomains[31]. We found herein that calcineurin activity was strongly increased in PAH-hPASMCs, and the knockdown of Orai1 strongly reduced this activity. Previous work on the MCT-induced PH model indicated that the calcineurin/NFAT axis is over-activated, modulating PASMCs proliferation and apoptosis[32]. Moreover, the calcineurin/NFAT axis is a significant regulator of cell migration[13]. In this study, we found an increase in PAH-hPASMCs motility, which was reversed in siOrai1-transfected PAH-hPASMCs. Moreover, we found that Orai1 upregulation in PAH-hPASMCs increases calcineurin activity, which regulates Orai1 expression.

Role of cardiac Orai1 in improving RV function

We recently demonstrated that Orai1 expression and function were enhanced in hypertrophied RV cardiomyocytes from MCT-rats[16]. Also, Orai1 overexpression/function is described in hypertrophied LV cardiomyocytes from LV pressure-overloaded mice[10], and genetic inactivation or pharmacological inhibition of Orai1 improves LV systolic function and Ca^{2+} handling[10]. Moreover, *in vitro*, in hypertrophied RV cardiomyocytes from MCT-rats, pharmacological inhibition of Orai1 normalized Ca^{2+} handling and cardiomyocyte contractility to control levels[16]. In the present study, we found that *in-vivo* inhibition of Orai1 by BTP2, JPIII, or 5J4 administration improved RV hypertrophy and RVSP in CH-, MCT- and Su/Hx rat

models, which could be explained by an improvement in pulmonary vascular remodeling and by the direct action of Orai1 blockade on RV cardiomyocyte function.

Pharmacological inhibition of Orai1 as a therapeutic option in PAH

Using siRNA or pharmacological Orai1 inhibition, we found that Orai1 inhibition reduced several pathological phenotypes of PAH-hPASMCs, including aberrant proliferation, exacerbated migration, and apoptosis resistance. This supports Orai1 as a relevant therapeutic target in PAH. Since the IC_{50} of BTP2 is between 100 and 590 nmol/L in several cell types[33], we used BTP2 at 1 µmol/L to avoid or minimize side effects. Indeed, at a higher concentration, BTP2 inhibits transient receptor potential (TRP) canonical 3 (TRPC3)-mediated Ca^{2+} entry in TRPC3-expressing HEK293 cells with an IC_{50} of 4 µmol/L[33]. In lymphocytes, BTP2 also dose-dependently enhances the function of TRP melastatin 4, which induces lymphocyte depolarization[34]. Also, in T lymphocytes, BTP2 inhibits TRPC5 channels[35]. Our study did not detect TRPC5 expression in lung tissue or hPASMCs (data not shown), eliminating the possibility of potential side effects of BTP2 on TRPC5. Moreover, at 10 µmol/L, BTP2 was recently shown to reduce the function of Orai1, Orai2, and Orai3[36]. We found that 1 µmol/L BTP2 has similar effects on PAH-hPASMCs (SOCE amplitude, proliferation, apoptosis, and migration) than siOrai1 in transfected PAH-hPASMCs. Therefore, we conclude that 1 µmol/L BTP2 is an efficient dose for selective blockade of Orai1 in PAH-hPASMCs. Additionally, we used another selective Orai1 blocker, JPIII, based on the scaffold of the potent and selective blocker, Synta66[10]. JPIII did not modify the function of Orai3, TRPC5, TRPC6, TRPC4/C1, or TRPC5/C1 in HEK293 cells[10]. JPIII (0.5 µmol/L) recapitulates results obtained in *in-vitro* experiments with siOrai1 or after 1 µmol/L BTP2 application. Finally, we obtained similar in-vivo results with 5J4 application in MCT-rats, for which no side effects have been reported on other Ca^{2+} channels until now[17]to those obtained with BTP2 and JPIII application. These data

prove that targeting the Orai1 Ca^{2+} channel function could be a promising strategy for treating PAH.

Orai1 inhibitors in clinical trials: a chance for the PAH community?

Since the discovery of SOCE by Putney in 1986[37] and the following identification of Orai1 as the archetype of SOCE in 2006[6], Orai1 is considered as a plausible target in several pathological processes. Now, in addition to BTP2, JPIII, and 5J4 used in this study, the arsenal of pharmacological inhibitors of Orai1 has increased, including GSK-7975A, Synta66, PRCL02, RP3128, a monoclonal antibody against Orai1 (mAB 2C1.1), and Auxora[8,10]. Some compounds have reached clinical trials (Phase I/IIa) for severe plaque psoriasis, acute pancreatitis, and COVID-19 pneunomia[38,39]. Currently, the above-listed molecules seem to be well-tolerated in patients[8]. RP3128 has reached clinical trials (Phase I/IIa) for asthma[40]. Finally, PRCL02 entered into clinical trials for the treatment of plaque psoriasis[41]. Since we demonstrated that Orai1 contributes to PAH development, it would be interesting to test the different Orai1 inhibitors in PAH, especially since good safety in humans has been already demonstrated in several Phase I and II clinical trials. Using Orai1 inhibitors, we demonstrated that we might act on different PAH pathogeneses, including exacerbated proliferation, migration, apoptosis resistance, and PA constriction.

However, intracellular Ca^{2+} overload could be due to plasma membrane channels, including voltage-gated Ca^{2+} channels and non-voltage-gated Ca^{2+} channels. In the clinic PAH, L-type voltage-gated Ca^{2+} channel blockers, acting mainly on excessive PA vasoconstriction, are only effective for less than 10% of PAH patients[5]. As the archetype of SOC, the Orai1 channel appears to be a novel alternative to counteract intracellular Ca^{2+} overload in PAH by regulating cell function. Another essential advantage to inhibiting Orai1 is that most molecules tested in the preclinical models and clinical studies act on downstream proteins or at the end of cell signaling. Like Sotatercept therapy (which acts at the start of the TGFβ signaling cascade)[42],

Orai1 inhibition also acts at the beginning of the Ca^{2+} signaling. For all these reasons, and due to the existence of a safe Orai1 inhibitor, Orai1 blockade therapy should be tested in PAH patients.

In conclusion, our findings prove that Orai1 contributes to PAH development by regulating the aberrant PASMC phenotype, including hyper-proliferation, apoptosis resistance, excessive migration, and contraction. Our data suggest that pharmacological inhibition of Orai1 could be a relevant strategy to reduce pulmonary vascular remodeling in PAH once the safety of Orai1 inhibition is confirmed.

Acknowledgments- The authors thank Yvonne Dutheil from INSERM U999, Hopital Marie Lannelongue for all her help.

Sources of Funding- This study was supported by grants from the French National Institute for Health and Medical Research (INSERM), the Université Paris-Saclay, the Marie Lannelongue Hospital, and the French National Agency for Research (ANR) (grant no. ANR-18-CE14-0023 (KAPAH), and the British Heart Foundation (grant no. FS/16/42/32308 for E.W. and FS/18/12/33270 for M.B.). B.M. is supported by the Therapeutic Innovation Doctoral School (ED569). ANR-18-CE14-0023 supports H.L.R.

Disclosures- MH and DM have relationships with drug companies, including Actelion, Bayer, GSK, Novartis, and Pfizer. In addition to being investigators in trials involving these companies, other relationships include consultancy services and memberships to scientific advisory boards. The other authors have no conflicts of interest to declare.

References

1. Humbert M, Guignabert C, Bonnet S, Dorfmüller P, Klinger JR, Nicolls MR, Olschewski AJ, Pullamsetti SS, Schermuly RT, Stenmark KR, Rabinovitch M. Pathology and pathobiology of pulmonary hypertension: state of the art and research perspectives. *Eur Respir J*. 2019;53:1801887.

2. Simonneau G, Montani D, Celermajer DS, Denton CP, Gatzoulis MA, Krowka M, Williams PG, Souza R. Haemodynamic definitions and updated clinical classification of pulmonary hypertension. *Eur Respir J*. 2019;53.

3. Lau EMT, Giannoulatou E, Celermajer DS, Humbert M. Epidemiology and treatment of pulmonary arterial hypertension. *Nat Rev Cardiol*. 2017;14:603–614.

4. Berna-Erro A, Jardín I, Smani T, Rosado JA. Regulation of Platelet Function by Orai, STIM and TRP. *Adv Exp Med Biol*. 2016;898:157–181.

5. Masson B, Montani D, Humbert M, Capuano V, Antigny F. Role of Store-Operated Ca2+ Entry in the Pulmonary Vascular Remodeling Occurring in Pulmonary Arterial Hypertension. *Biomolecules*. 2021;11:1781.

6. Vig M, Peinelt C, Beck A, Koomoa DL, Rabah D, Koblan-Huberson M, Kraft S, Turner H, Fleig A, Penner R, Kinet J-P. CRACM1 is a plasma membrane protein essential for store-operated Ca2+ entry. *Science*. 2006;312:1220–1223.

7. Yeromin AV, Zhang SL, Jiang W, Yu Y, Safrina O, Cahalan MD. Molecular identification of the CRAC channel by altered ion selectivity in a mutant of Orai. *Nature*. 2006;443:226–229.

8. Stauderman KA. CRAC channels as targets for drug discovery and development. *Cell Calcium*. 2018;74:147–159.

9. Sweeney ZK, Minatti A, Button DC, Patrick S. Small-molecule inhibitors of store-operated calcium entry. *ChemMedChem*. 2009;4:706–718.

10. Bartoli F, Bailey MA, Rode B, Mateo P, Antigny F, Bedouet K, Gerbaud P, Gosain R, Plante J, Norman K, Gomez S, Lefebvre F, Rucker-Martin C, Ainscough JFX, Kearney MT, Bruns A-F, Shi J, Appleby HL, Young RS, Shawer HM, Debant M, Gomez A-M, Beech DJ, Foster R, Benitah J-P, Sabourin J. Orai1 Channel Inhibition Preserves Left Ventricular Systolic Function and Normal Ca2+ Handling After Pressure Overload. *Circulation*. 2020;141:199–216.

11. Wang X, Wang Y, Zhou Y, Hendron E, Mancarella S, Andrake MD, Rothberg BS, Soboloff J, Gill DL. Distinct Orai-coupling domains in STIM1 and STIM2 define the Orai-activating site. *Nat Commun*. 2014;5:3183.

12. Sankhe S, Manousakidi S, Antigny F, Arthur Ataam J, Bentebbal S, Ruchon Y, Lecerf F, Sabourin J, Price L, Fadel E, Dorfmüller P, Eddahibi S, Humbert M, Perros F, Capuano V. T-type Ca2+channels elicit pro-proliferative and anti-apoptotic responses through impaired PP2A/Akt1 signaling in PASMCs from patients with pulmonary arterial hypertension. *Biochim Biophys Acta*. 2017;1864:1631–1641.

13. Villalobo A, Berchtold MW. The Role of Calmodulin in Tumor Cell Migration, Invasiveness, and Metastasis. *Int J Mol Sci*. 2020;21.

14. Le Ribeuz H, To L, Ghigna M-R, Martin C, Nagaraj C, Dreano E, Rucker-Martin C, Girerd B, Bouliguan J, Pechoux C, Lambert M, Boet A, Issard J, Mercier O, Hoetzenecker K, Manoury B, Becq F, Burgel P-R, Cottart C-H, Olschewski A, Sermet-Gaudelus I, Perros F, Humbert M, Montani D, Antigny F. Involvement of CFTR in the pathogenesis of pulmonary arterial hypertension. *Eur Respir J*. 2021;

15. Rimessi A, Patergnani S, Bonora M, Wieckowski MR, Pinton P. Mitochondrial Ca(2+) Remodeling is a Prime Factor in Oncogenic Behavior. *Front Oncol*. 2015;5:143.

16. Sabourin J, Boet A, Rucker-Martin C, Lambert M, Gomez A-M, Benitah J-P, Perros F, Humbert M, Antigny F. Ca2+ handling remodeling and STIM1L/Orai1/TRPC1/TRPC4 upregulation in monocrotaline-induced right ventricular hypertrophy. *J Mol Cell Cardiol*. 2018;118:208–224.

17. Kim K-D, Srikanth S, Tan Y-V, Yee M-K, Jew M, Damoiseaux R, Jung ME, Shimizu S, An DS, Ribalet B, Waschek JA, Gwack Y. Calcium Signaling via Orai1 Is Essential for Induction of the Nuclear Orphan Receptor Pathway To Drive Th17 Differentiation. *J Immunol*. 2014;192:110–122.

18. Potier M, Gonzalez JC, Motiani RK, Abdullaev IF, Bisaillon JM, Singer HA, Trebak M. Evidence for STIM1- and Orai1-dependent store-operated calcium influx through ICRAC in vascular smooth muscle cells: role in proliferation and migration. *FASEB J Off Publ Fed Am Soc Exp Biol*. 2009;23:2425–2437.

19. Wang Y, He J, Jiang H, Zhang Q, Yang H, Xu X, Zhang C, Xu C, Wang J, Lu W. Nicotine enhances store-operated calcium entry by upregulating HIF-1α and SOCC components in non-small cell lung cancer cells. *Oncol Rep*. 2018;40:2097–2104.

20. Lambert M, Capuano V, Boet A, Tesson L, Bertero T, Nakhleh MK, Remy S, Anegon I, Pechoux C, Hautefort A, Rucker-Martin C, Manoury B, Domergue V, Mercier O, Girerd B, Montani D, Perros F, Humbert M, Antigny F. Characterization of Kcnk3-Mutated Rat, a Novel Model of Pulmonary Hypertension. *Circ Res*. 2019;125:678–695.

21. Ogawa A, Firth AL, Smith KA, Maliakal MV, Yuan JX-J. PDGF enhances store-operated Ca2+ entry by upregulating STIM1/Orai1 via activation of Akt/mTOR in human pulmonary arterial smooth muscle cells. *Am J Physiol Cell Physiol*. 2012;302:C405-411.

22. Flourakis M, Lehen'kyi V, Beck B, Raphaël M, Vandenberghe M, Abeele FV, Roudbaraki M, Lepage G, Mauroy B, Romanin C, Shuba Y, Skryma R, Prevarskaya N. Orai1 contributes to the establishment of an apoptosis-resistant phenotype in prostate cancer cells. *Cell Death Dis*. 2010;1:e75.

23. Liang S-J, Zeng D-Y, Mai X-Y, Shang J-Y, Wu Q-Q, Yuan J-N, Yu B-X, Zhou P, Zhang F-R, Liu Y-Y, Lv X-F, Liu J, Ou J-S, Qian J-S, Zhou J-G. Inhibition of Orai1 Store-Operated Calcium Channel Prevents Foam Cell Formation and Atherosclerosis. *Arterioscler Thromb Vasc Biol*. 2016;36:618–628.

24. Vacher P, Vacher A-M, Pineau R, Latour S, Soubeyran I, Pangault C, Tarte K, Soubeyran P, Ducret T, Bresson-Bepoldin L. Localized Store-Operated Calcium Influx Represses CD95-Dependent Apoptotic Effects of Rituximab in Non-Hodgkin B Lymphomas. *J Immunol Baltim Md 1950*. 2015;195:2207–2215.

25. Horton JS, Buckley CL, Alvarez EM, Schorlemmer A, Stokes AJ. The calcium release-activated calcium channel Orai1 represents a crucial component in hypertrophic compensation and the development of dilated cardiomyopathy. *Channels Austin Tex*. 2014;8:35–48.

26. Yue J, López JM. Understanding MAPK Signaling Pathways in Apoptosis. *Int J Mol Sci*. 2020;21.

27. Wagner EF, Nebreda AR. Signal integration by JNK and p38 MAPK pathways in cancer development. *Nat Rev Cancer*. 2009;9:537–549.

28. Rao A, Luo C, Hogan PG. Transcription factors of the NFAT family: regulation and function. *Annu Rev Immunol*. 1997;15:707–747.

29. Gallo EM, Canté-Barrett K, Crabtree GR. Lymphocyte calcium signaling from membrane to nucleus. *Nat Immunol*. 2006;7:25–32.

30. Feske S, Gwack Y, Prakriya M, Srikanth S, Puppel S-H, Tanasa B, Hogan PG, Lewis RS, Daly M, Rao A. A mutation in Orai1 causes immune deficiency by abrogating CRAC channel function. *Nature*. 2006;441:179–185.

31. Kar P, Lin Y-P, Bhardwaj R, Tucker CJ, Bird GS, Hediger MA, Monico C, Amin N, Parekh AB. The N terminus of Orai1 couples to the AKAP79 signaling complex to drive NFAT1 activation by local Ca2+ entry. *Proc Natl Acad Sci U S A*. 2021;118.

32. He R-L, Wu Z-J, Liu X-R, Gui L-X, Wang R-X, Lin M-J. Calcineurin/NFAT Signaling Modulates Pulmonary Artery Smooth Muscle Cell Proliferation, Migration and Apoptosis in Monocrotaline-Induced Pulmonary Arterial Hypertension Rats. *Cell Physiol Biochem Int J Exp Cell Physiol Biochem Pharmacol*. 2018;49:172–189.

33. He L-P, Hewavitharana T, Soboloff J, Spassova MA, Gill DL. A functional link between store-operated and TRPC channels revealed by the 3,5-bis(trifluoromethyl)pyrazole derivative, BTP2. *J Biol Chem*. 2005;280:10997–11006.

34. Takezawa R, Cheng H, Beck A, Ishikawa J, Launay P, Kubota H, Kinet J-P, Fleig A, Yamada T, Penner R. A pyrazole derivative potently inhibits lymphocyte Ca2+ influx and cytokine production by facilitating transient receptor potential melastatin 4 channel activity. *Mol Pharmacol*. 2006;69:1413–1420.

35. Zitt C, Strauss B, Schwarz EC, Spaeth N, Rast G, Hatzelmann A, Hoth M. Potent inhibition of Ca2+ release-activated Ca2+ channels and T-lymphocyte activation by the pyrazole derivative BTP2. *J Biol Chem*. 2004;279:12427–12437.

36. Zhang X, Xin P, Yoast RE, Emrich SM, Johnson MT, Pathak T, Benson JC, Azimi I, Gill DL, Monteith GR, Trebak M. Distinct pharmacological profiles of ORAI1, ORAI2, and ORAI3 channels. *Cell Calcium*. 2020;91:102281.

37. Putney JW. A model for receptor-regulated calcium entry. *Cell Calcium*. 1986;7:1–12.

38. CalciMedica, Inc. An Open-Label, Dose-Response Study of CM4620 Injectable Emulsion (CM4620-IE) in Patients With Acute Pancreatitis and Accompanying Systemic Inflammatory Response Syndrome (SIRS) [Internet]. clinicaltrials.gov; 2019 [cited 2021 Apr 25]. Available from: https://clinicaltrials.gov/ct2/show/NCT03401190

39. Miller J, Bruen C, Schnaus M, Zhang J, Ali S, Lind A, Stoecker Z, Stauderman K, Hebbar S. Auxora versus standard of care for the treatment of severe or critical COVID-19 pneumonia: results from a randomized controlled trial. *Crit Care Lond Engl*. 2020;24:502.

40. Rhizen Pharmaceuticals SA. A Phase I/IIa, Randomized, Double-blind, Placebo Controlled Study to Evaluate the Safety, and Pharmacokinetics of Single and Multiple Ascending Dose of RP3128 in HV and Effect on LAR to Allergen Challenge in Mild Asthmatics [Internet]. clinicaltrials.gov; 2019 [cited 2021 Apr 25]. Available from: https://clinicaltrials.gov/ct2/show/NCT02958982

41. PRCL Research Inc. Randomized, Double Blind, Placebo Controlled, Incomplete Crossover Single Oral Dose Escalation of PRCL-02 in Normal Healthy Volunteers (Part A) and Multiple Oral Dose Escalation in Normal Healthy Volunteers (Part B) and in Chronic Plaque Psoriasis Patients (Part C) [Internet]. clinicaltrials.gov; 2018 [cited 2021 Apr 25]. Available from: https://clinicaltrials.gov/ct2/show/NCT03062618

42. Humbert M, McLaughlin V, Gibbs JSR, Gomberg-Maitland M, Hoeper MM, Preston IR, Souza R, Waxman A, Escribano Subias P, Feldman J, Meyer G, Montani D, Olsson KM, Manimaran S, Barnes J, Linde PG, de Oliveira Pena J, Badesch DB, PULSAR Trial Investigators. Sotatercept for the Treatment of Pulmonary Arterial Hypertension. *N Engl J Med*. 2021;384:1204–1215.

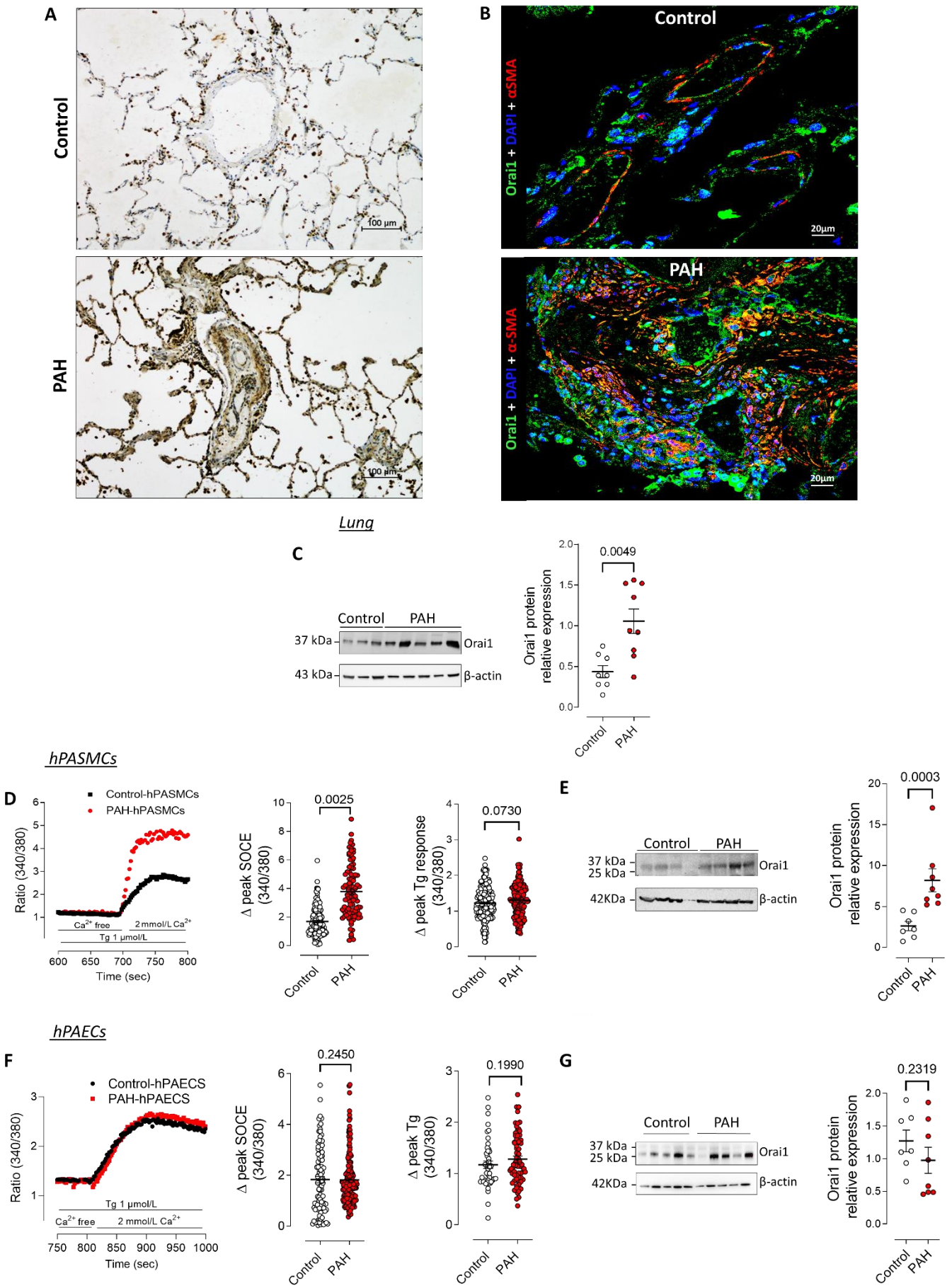
A
Control
PAH
100 µm
100 µm
B
Control
Orai1 + DAPI + αSMA
20µm
PAH
Orai1 + DAPI + α-SMA
20µm
Lung
C
Control
PAH
37 kDa
Orai1
43 kDa
β-actin
Orai1 protein relative expression
0.0049
Control
PAH
hPASMCs
D
Control-hPASMCs
PAH-hPASMCs
Ratio (340/380)
Ca2+ free
2 mmol/L Ca2+
Tg 1 µmol/L
Time (sec)
Δ peak SOCE (340/380)
0.0025
Control
PAH
Δ peak Tg response (340/380)
0.0730
Control
PAH
E
Control
PAH
37 kDa
25 kDa
Orai1
42KDa
β-actin
Orai1 protein relative expression
0.0003
Control
PAH
hPAECs
F
Control-hPAECS
PAH-hPAECS
Ratio (340/380)
Tg 1 µmol/L
Ca2+ free
2 mmol/L Ca2+
Time (sec)
Δ peak SOCE (340/380)
0.2450
Control
PAH
Δ peak Tg (340/380)
0.1990
Control
PAH
G
Control
PAH
37 kDa
25 kDa
Orai1
42KDa
β-actin
Orai1 protein relative expression
0.2319
Control
PAH

Figure 1

Figure 1: Increased expression of Orai1 and SOCE in PAH-hPASMCs. (A) Expression and localization of Orai1 by immunohistochemistry in paraffin-embedded lung sections from control and PAH patients. Bar graph = 100 μm. (B) Expression and localization of Orai1 by immunofluorescence staining on paraffin-embedded lung sections from control and PAH patients (Orai1 staining (green) and αSMA staining (Red)). Bar graph = 20 μm. (C) Immunoblot of Orai1 expression and quantification in lungs from control and PAH patients (n = 7 for control and 8 for PAH). (F) SOCE in control hPAECs and PAH-hPAECs. (D) Quantification of SOCE amplitude and quantification of Tg-induced Ca^{2+} release (N = 9 patients; n = 129 control cells and 101 PAH cells). (E) Immunoblot and quantification of Orai1 expression in PAH-hPAECs (n = 7 for control and 8 for PAH). (D) SOCE in control-hPASMCs and PAH-hPASMCs. Quantification of SOCE amplitude and quantification of Thapsigargin (Tg)-induced Ca^{2+} release (N = 7 7 patients; n = 107 control cells and 153 PAH cells). (G) Immunoblot and quantification of Orai1 expression in PAH-hPASMCs (n = 7 for control and 8 for PAH). Statistical tests and exact P values are provided in Table S5.

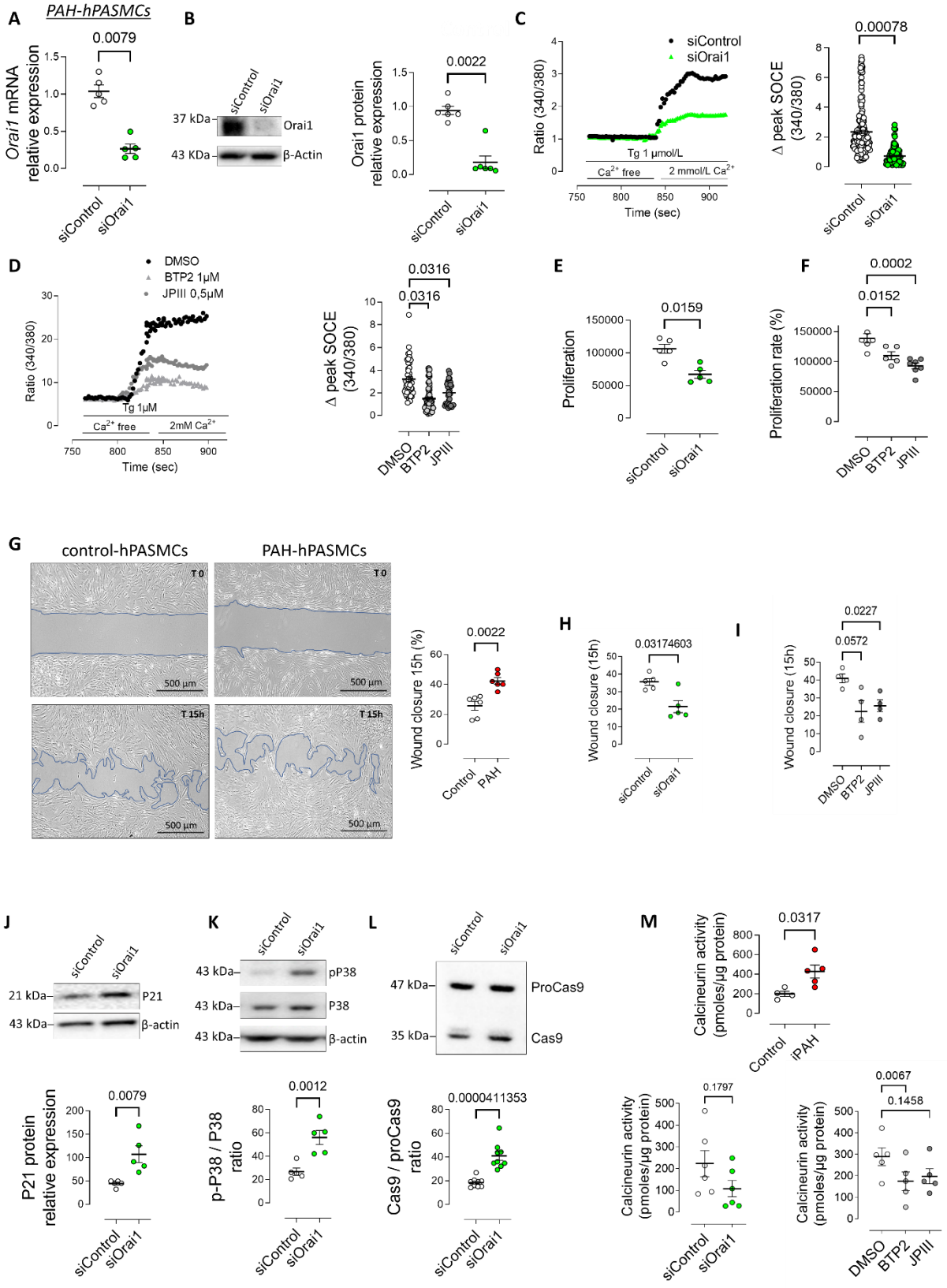
A
PAH-hPASMCs
0.0079
Orai1 mRNA relative expression
siControl
siOrai1
B
siControl
siOrai1
37 kDa
Orai1
43 KDa
β-Actin
0.0022
Orai1 protein relative expression
C
siControl
siOrai1
Ratio (340/380)
Tg 1 µmol/L
Ca2+ free
2 mmol/L Ca2+
Time (sec)
0.00078
Δ peak SOCE (340/380)
D
DMSO
BTP2 1µM
JPIII 0,5µM
Ratio (340/380)
Tg 1µM
Ca2+ free
2mM Ca2+
Time (sec)
0.0316
0.0316
Δ peak SOCE (340/380)
DMSO
BTP2
JPIII
E
0.0159
Proliferation
F
0.0002
0.0152
Proliferation rate (%)
G
control-hPASMCs
PAH-hPASMCs
T 0
T 15h
500 µm
0.0022
Wound closure 15h (%)
Control
PAH
H
0.03174603
Wound closure (15h)
I
0.0227
0.0572
Wound closure (15h)
J
siControl
siOrai1
21 kDa
P21
43 kDa
β-actin
0.0079
P21 protein relative expression
K
43 kDa
pP38
P38
β-actin
0.0012
p-P38 / P38 ratio
L
47 kDa
ProCas9
35 kDa
Cas9
0.0000411353
Cas9 / proCas9 ratio
M
0.0317
Calcineurin activity (pmoles/µg protein)
Control
iPAH
0.1797
0.0067
0.1458
DMSO
BTP2
JPIII

Figure 2

Figure 2: Increase in Orai1 expression in PAH-hPASMCs is associated with an exaggerated SOCE, proliferation, migration, higher an apoptosis resistance, and calcineurin activity. (A) PAH-hPASMCs were transfected with siRNA against Orai1, and knockdown efficiency was assessed by RT-qPCR (n = 5 for each condition) (B) and immunoblot (n = 6 for each condition). (C) Consequence of Orai1 knockdown in PAH-hPASMCs on SOCE amplitude (N = 7 patients; n = 174 siControl cells and 121 siOrai1 cells). (D) Consequence of Orai1 inhibition using 1 µmol/L BTP2 or 0.5 µmol/L JPIII on SOCE amplitude (N = 5 different patients; DMSO 45 cells, BTP2 61 cells and JPIII 32 cells). (E) Consequence of Orai1 knockdown on the proliferation rate (BrdU assay) of PAH-hPASMCs (n = 9 patients). (F) Consequence of pharmacological inhibition of Orai1 on the proliferation rate of PAH-hPASMCs treated for 24 h with DMSO or BTP2 (1 µmol/L) or JPIII (0.5 µmol/L) (n = 5 patients for DMSO and BTP2 and 3 patients for JPIII). (G) Wound-closure images (15 h after initiation) and percentage wound closure in control hPASMCs and PAH-hPASMCs (n = 4 patients for each condition). (H) Consequence of Orai1 knockdown on PAH-hPASMC motility/invasion (n = 5 patients). (I) Consequence of Orai1 inhibition PAH-hPASMC mobility/invasion (n = 4 for each condition). (J-L) Immunoblots and quantification of P21 (n = 5 patients), pP38 and P38 (n = 5 patients), proCaspase 9 and cleaved Caspase 9 (n = 9 patients) in PAH-hPASMCs transfected with siControl or siOrai1. (M) Quantification of calcineurin activity in control-hPASMCs and PAH-hPASMCs (n = 5 patients). Consequence of Orai1 knockdown (n = 5 for control and 6 for PAH patients) or inhibition (n = 5 patients) in PAH-hPASMCs on calcineurin activity. Statistical tests and exact P values are provided in Table S5.

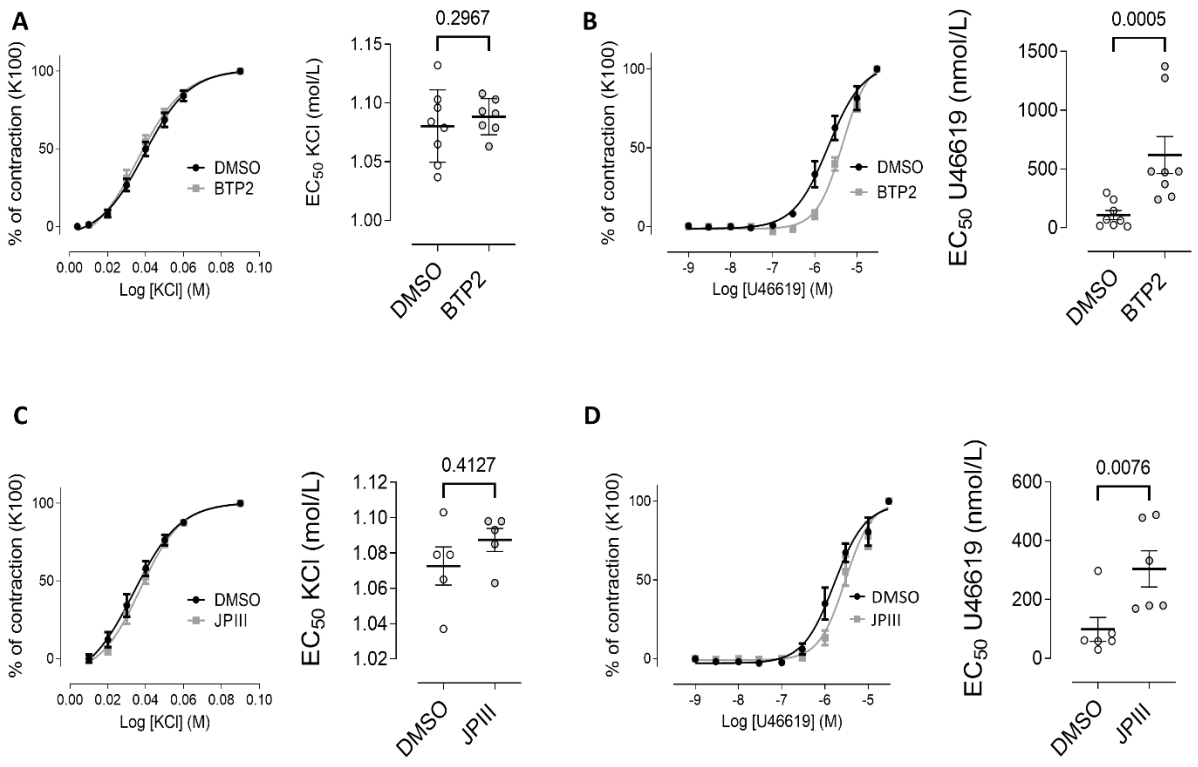

Figure 3

Figure 3: The Orai1 channel contributes to PA contraction. (A, left panel) A dose-response curve (normalized to K100) was established by applying increasing concentrations of KCl to isolated human PAs from control subjects in the presence of DMSO or 1 µmol/L BTP2. (A, right panel) Corresponding quantification of EC_{50} (n = 8 patients). (B, left panel) A dose-response curve (normalized to K100) was established by applying increasing concentrations of U46619 (a thromboxane A2 mimetic) on isolated human PAs from control subjects in the presence of DMSO or 1 µmol/L BTP2. (B, right panel) Corresponding quantification of EC_{50} values (n = 8 patients). (C, left panel) A dose-response curve (normalized to K100) was established by applying increasing concentrations of KCl to isolated human PAs from control subjects in the presence of DMSO or 1 µmol/L JPIII. (A, right panel) Corresponding quantification of EC50 (n = 5 patients). (D, left panel) A dose-response curve (normalized to K100) was established by applying increasing concentrations of U46619 on isolated human

PAs from control subjects in the presence of DMSO or 1 µmol/L JPIII. (D, right panel) Corresponding quantification of EC50 values (n = 6 patients). Statistical tests and exact P values are provided in Table S5.

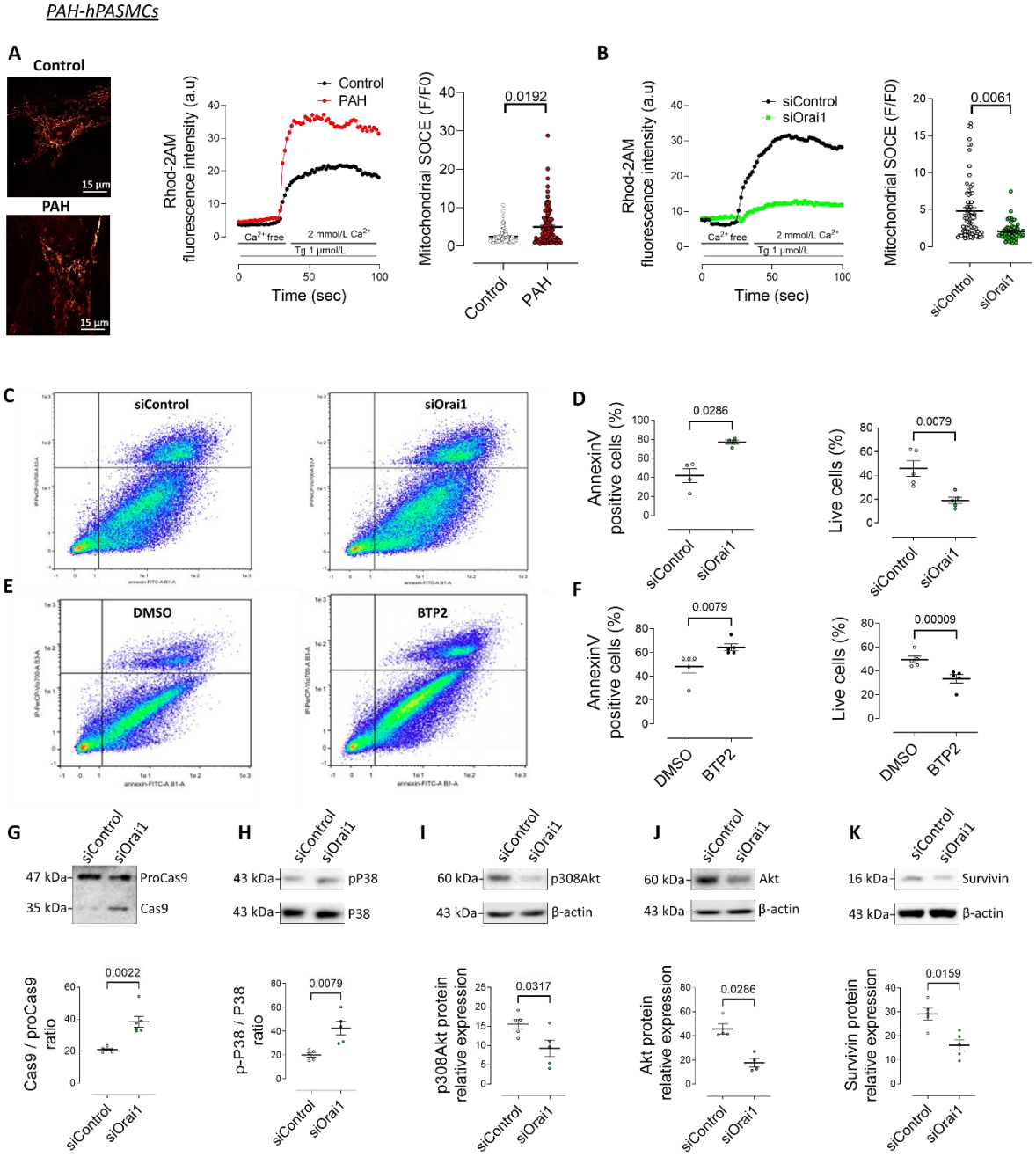

Figure 4

Figure 4: Knockdown of Orai1 reduces mitochondrial Ca^{2+} uptake and enhances apoptosis in PAH-hPASMCs exposed to staurosporine. (A) Measurement of mitochondrial Ca^{2+} uptake using Rhod2-AM fluorescent Ca^{2+} probes and quantification of mitochondrial Ca^{2+} entry during SOCE in control and PAH-hPASMCs (N = 7 patients; n = 88 mitochondria for control and 98 for PAH). (B) Consequence of the Orai1 knockdown on mitochondrial Ca^{2+} uptake during SOCE in PAH-hPASMCs (N = 7 patients; n = 70 mitochondria for control and 50 for PAH)). (C) Dot plots of Annexin V+PI dual-labeling in siControl- or siOrai1-transfected PAH-hPASMCs exposed to 50 nmol/L staurosporine overnight. (D) Percentage of Annexin V-positive and live PAH-hPASMCs transfected with siControl or siOrai1 (n = 5 patients). (E) Dot plots of Annexin V and PI dual-labeling of PAH-hPASMCs exposed overnight to 50 nmol/L staurosporine with DMSO or BTP2. (F) Percentage of Annexin V-positive or live PAH-hPASMCs treated with DMSO or BTP2 (n = 5 patients). (J-K) Immunoblots and quantification of Caspase 9/pro-Caspase 9 (n = 6 patients), p-P38/P38 (n = 5 patients), p308Akt (n = 5 patients), Akt (n = 4 patients), and survivin in PAH-hPASMCs transfected with siControl or siOrai1 and exposed overnight to 50 nmol/L staurosporine. Statistical tests and exact P values are provided in Table S5.

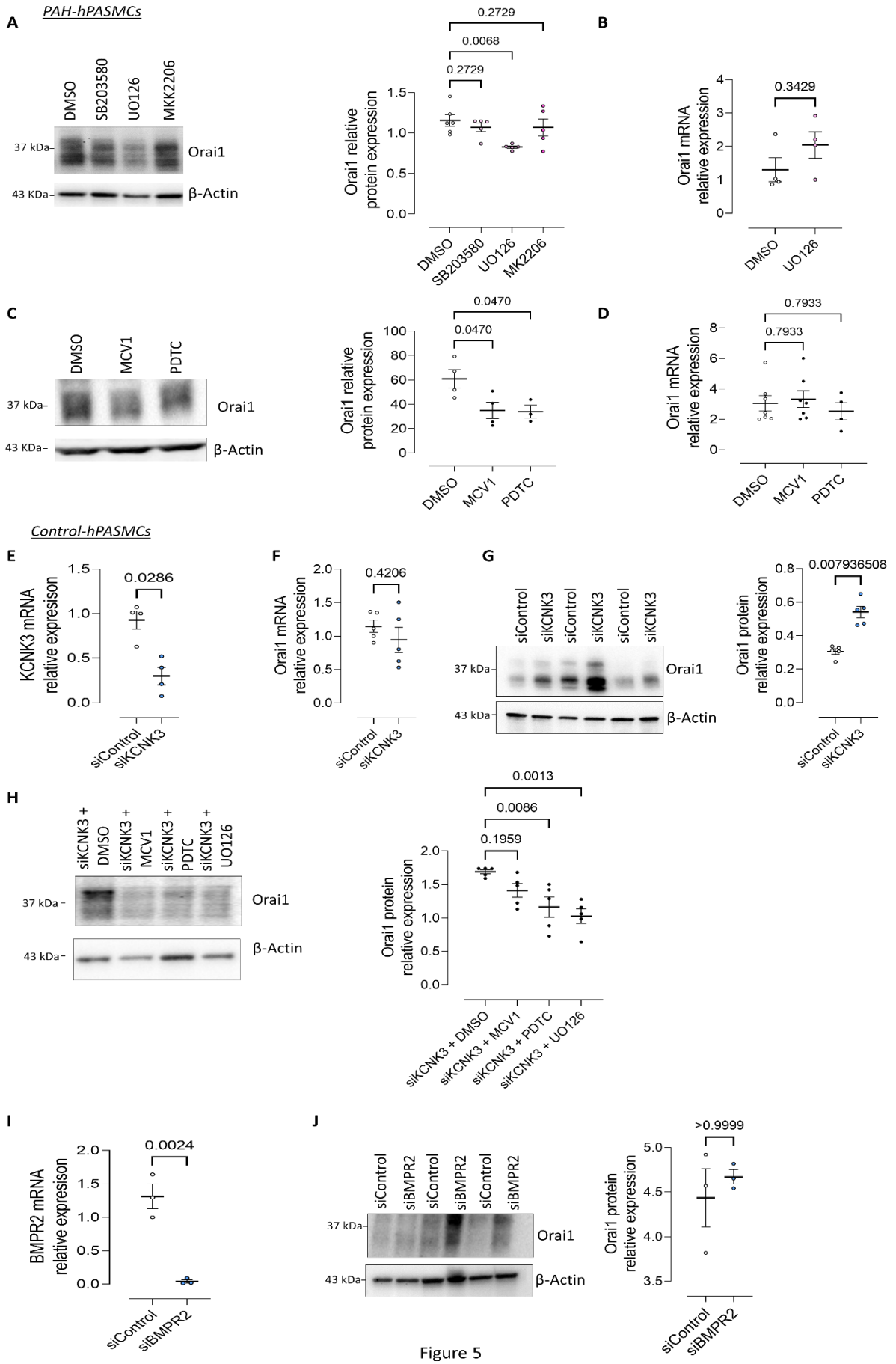
PAH-hPASMCs
A
DMSO
SB203580
UO126
MKK2206
37 kDa
Orai1
43 KDa
β-Actin
Orai1 relative protein expression
0.2729
0.0068
0.2729
DMSO
SB203580
UO126
MK2206
B
Orai1 mRNA relative expression
0.3429
DMSO
UO126
C
DMSO
MCV1
PDTC
37 kDa
Orai1
43 KDa
β-Actin
Orai1 relative protein expression
0.0470
0.0470
DMSO
MCV1
PDTC
D
Orai1 mRNA relative expression
0.7933
0.7933
DMSO
MCV1
PDTC
Control-hPASMCs
E
KCNK3 mRNA relative expresison
0.0286
siControl
siKCNK3
F
Orai1 mRNA relative expression
0.4206
siControl
siKCNK3
G
siControl
siKCNK3
siControl
siKCNK3
siControl
siKCNK3
37 kDa
Orai1
43 kDa
β-Actin
Orai1 protein relative expression
0.007936508
siControl
siKCNK3
H
siKCNK3 + DMSO
siKCNK3 + MCV1
siKCNK3 + PDTC
siKCNK3 + UO126
37 kDa
Orai1
43 kDa
β-Actin
Orai1 protein relative expression
0.0013
0.0086
0.1959
siKCNK3 + DMSO
siKCNK3 + MCV1
siKCNK3 + PDTC
siKCNK3 + UO126
I
BMPR2 mRNA relative expresison
0.0024
siControl
siBMPR2
J
siControl
siBMPR2
siControl
siBMPR2
siControl
siBMPR2
37 kDa
Orai1
43 kDa
β-Actin
Orai1 protein relative expression
>0.9999
siControl
siBMPR2

Figure 5

Figure 5: MEK1/2, NFAT, and NF-κB upregulate Orai1 expression or function in hPASMCs. (A) Immunoblots and quantification of Orai1 in PAH-hPASMCs treated 48h with P38 inhibitor (SB203580 1 µmol/L), MEK1/2 inhibitor (UO126, 1 µmol/L), and AKT inhibitor (MK2206 1 µmol/L). (B) Quantification of Orai1 mRNA expression in PAH-hPASMCs treated with DMSO or UO126 (n = 4 for each condition). (C) Immunoblots and quantification of Orai1 in PAH-hPASMCs treated 48h with NFAT inhibitor (MCV1 1 µmol/L) and NF-κB inhibitor (PDTC, 1 µmol/L). (D) Quantification of Orai1 mRNA expression in PAH-hPASMCs treated with DMSO, MCV1 or PDTC (n = 7 for DMSO and MCV1 and 4 for PDTC). Consequence of the KCNK3 knockdown on KCNK3 (n = 4 patients) (E) and Orai1 (n = 5 patients) (F) mRNA expression in control hPASMCs. (G) Consequence of KCNK3 knockdown on Orai1 protein expression (n = 5 patients). (H) Quantification of Orai1 protein expression in control-hPASMCs transfected with siKCNK3 in the presence of DMSO, MCV1, PTDC, and UO126 (n = 5 patients). (I) Consequence of the BMPR2 knockdown on BMPR2. (J) The consequence of BMPR2 knockdown on Orai1 protein expression (n = 5 patients). Statistical tests and exact P values are provided in Table S5.

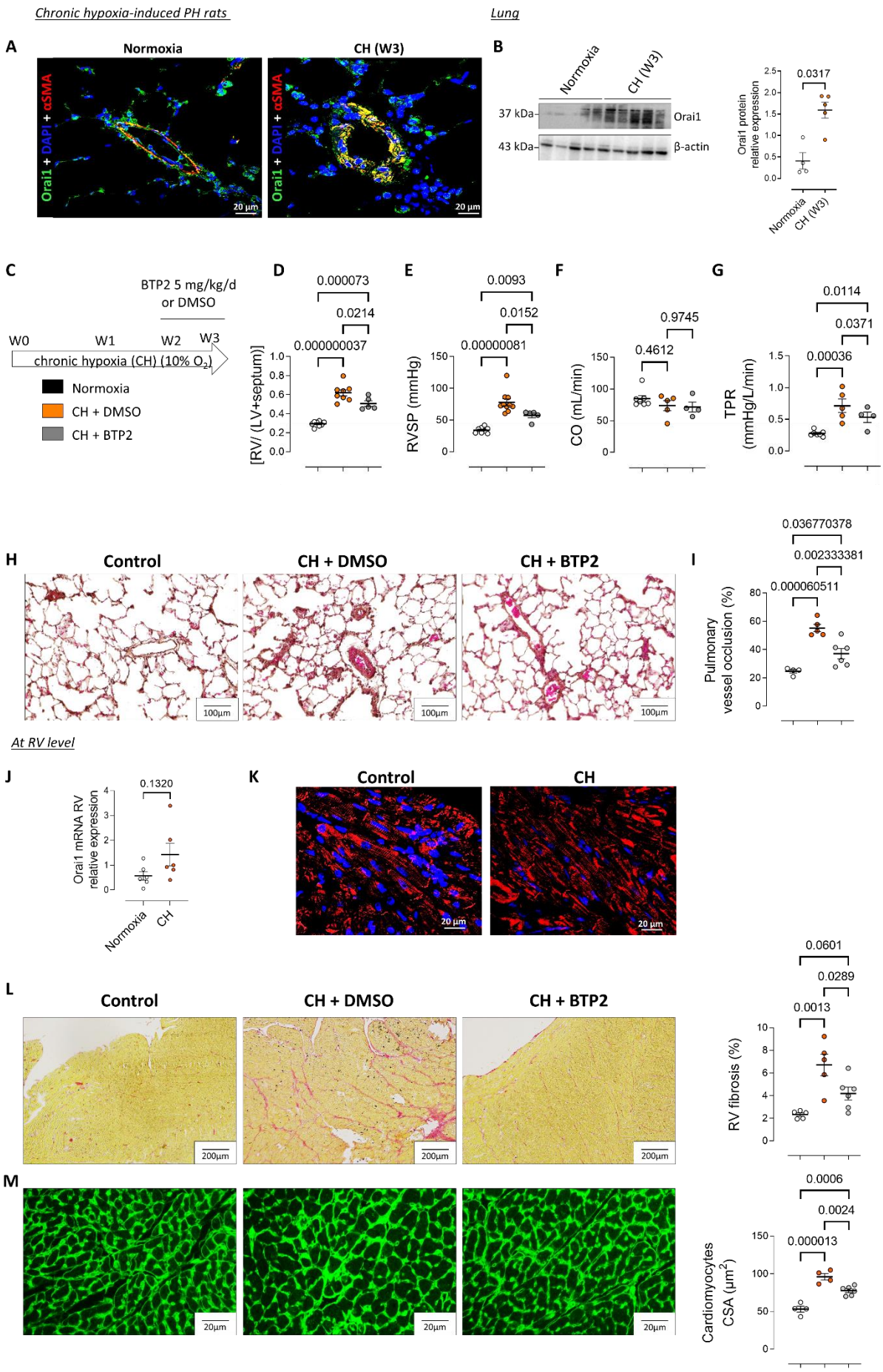
Chronic hypoxia-induced PH rats
Lung
A
Normoxia
CH (W3)
Orai1 + DAPI + αSMA
20 µm
B
Normoxia
CH (W3)
37 kDa
Orai1
43 kDa
β-actin
Orai1 protein relative expression
0.0317
C
BTP2 5 mg/kg/d or DMSO
W0
W1
W2
W3
chronic hypoxia (CH) (10% O2)
Normoxia
CH + DMSO
CH + BTP2
D
[RV/ (LV+septum)]
0.000073
0.0214
0.000000037
E
RVSP (mmHg)
0.0093
0.0152
0.00000081
F
CO (mL/min)
0.9745
0.4612
G
TPR (mmHg/L/min)
0.0114
0.0371
0.00036
H
Control
CH + DMSO
CH + BTP2
100µm
I
Pulmonary vessel occlusion (%)
0.036770378
0.002333381
0.000060511
At RV level
J
Orai1 mRNA RV relative expression
0.1320
Normoxia
CH
K
Control
CH
20 µm
L
Control
CH + DMSO
CH + BTP2
200µm
RV fibrosis (%)
0.0601
0.0289
0.0013
M
20µm
Cardiomyocytes CSA (µm2)
0.0006
0.0024
0.000013

Figure 6

Figure 6: In-vivo pharmacological inhibition of Orai1 with BTP2 reduces the development of chronic hypoxia (CH)-induced PH at pulmonary and RV levels. (A) Localization of Orai1 expression by immunofluorescence staining of paraffin-embedded lung sections from control- and CH-rats after three weeks (W3) hypoxia. In PAs from control rats, Orai1 staining (green) was localized to PASMCs (red). Bar graph = 20 µm. (B) Immunoblot images and quantification of Orai1 expression in lung tissue from control- and CH-rats (n = 4 for the Normoxia group and 5 for the CH group). (C) *In-vivo* experimental design. Rats were maintained in CH for 3 weeks, and BTP2 (5 mg/kg/day) or DMSO was administered during the 7 days between week 2 (W2) and W3 by intraperitoneal injection. (D) Fulton's index (RV ÷ (LV + septum)) (n = 8 for the Normoxia and CH + DMSO group and 5 for the CH + BTP2 group). (E) RVSP in mmHg (n = 8 for the Normoxia group, 10 for the CH + DMSO group and 5 for the CH + BTP2 group). (F) CO in mL/min (n = 7 for the Normoxia group, 5 for the CH + DMSO group and 4 for the CH + BTP2 group). (G) TPR (n = 7 for the Normoxia group, 5 for the CH + DMSO group and 4 for the CH + BTP2 group). (H) Hematoxylin/eosin/Safran staining of paraffin-embedded lung sections from the control, CH + DMSO, and CH + BTP2 groups. (I) Pulmonary vessel occlusion (%) (n = 4 for the Normoxia group, 5 for the CH + DMSO group and 6 for the CH + BTP2 group). (J) Quantification of Orai1 mRNA expression in RV tissues from control and CH rats (n = 5 for each condition). (K) Localization of Orai1 expression by immunofluorescence staining of paraffin-embedded RV sections from control and CH rats. Orai1 staining (red) and nucleus (DAPI in blue). (L) Interstitial fibrosis was identified with Sirius red staining in the RV compartment from control, CH + DMSO, and CH + BTP2 rats (at W3). Quantification of the percentage of fibrosis in RV tissue (n = 10 images per rat from 5 different rats for the Normoxia and CH + DMSO group and 6 different rats for the CH-+ BTP2 group). (M) Immunofluorescence images of RV sections stained with FITC-conjugated wheat germ agglutinin (WGA, 50 µg/mL, green). Scale bar, 25 µm. Quantification of cardiomyocytes cross-

section area (CSA, n = 30 cardiomyocytes measurement per rat from 4 different rats for the Normoxia and CH + DMSO group and 6 different rats for the CH-+ BTP2 group). Statistical tests and exact P values are provided in Table S5.

MCT induced PH rats

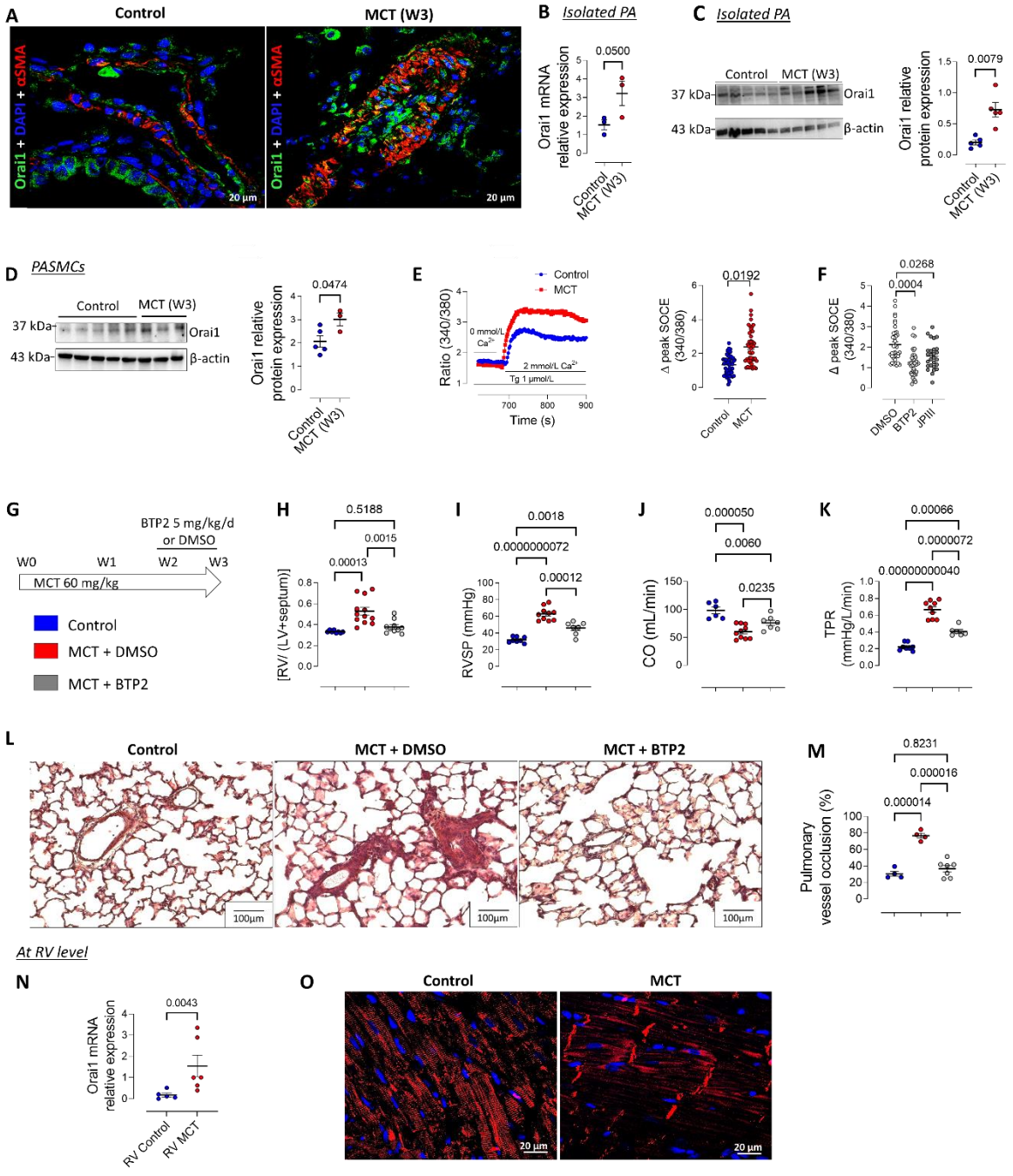

Figure 7

Figure 7: In-vivo pharmacological inhibition of Orai1 with BTP2 reduces SOCE in MCT-PASMCs and the development of MCT-induced PH at pulmonary and RV levels. (A) Localization of Orai1 expression by immunofluorescence staining of paraffin-embedded lung sections from control and MCT rats at three weeks (W3). In PAs from control rats, Orai1 staining (green) was localized in PASMCs (red). Bar graph = 20 µm. (B) Quantification of Orai1 mRNA expression in isolated PAs from control and MCT-rats (n = 4 rats for each condition). (C) Immunoblot images and quantification of Orai1 in PAs from control and MCT-rats. (n = 4 rats per condition). (D) Immunoblot images and quantification of Orai1 in PASMCs from control and MCT rats (n = 5 Control and 3 MCT rats). (E) SOCE and SOCE amplitude in PASMCs from control and MCT rats (N = 5 Control and 3 MCT rats; n = 51 cells for the Control condition and 47 for the MCT condition). (F) Consequence of Orai1 inhibition (BTP2 or JPIII) on SOCE in PASMCs from MCT rats (N = 3 rats for each condition; n = 38 cells for the DMSO condition, 34 for the BTP2 condition and 27 for the JPIII condition). (G) *In-vivo* experimental design. Rats have treated with one MCT subcutaneous injection at week 0 (W0) (60mg/kg). BTP2 (5 mg/kg/day) or DMSO was administered 7 days from week 2 (W2) to W3 by intraperitoneal injection. (H) Fulton's index (n = 8 for the Control group, 12 for the MCT + DMSO group and 10 for the MCT + BTP2 group), (I) RVSP (n = 8 for the Control group, 10 for the MCT + DMSO group and 7 for the MCT + BTP2 group), (J) CO (n = 7 for the Control group, 10 for the MCT + DMSO group and 7 for the MCT + BTP2 group) and (K) TPR (n = 7 for the Control group, 10 for the MCT + DMSO group and 7 for the MCT + BTP2 group). (L) Hematoxylin/eosin/Safran staining of paraffin-embedded lung sections from the control, MCT + DMSO, and MCT + BTP2 groups. (M) Pulmonary vessel occlusion (%) (n = 4 for the Control group, 4 for the MCT + DMSO group and 7 for the MCT + BTP2 group). (N) Quantification of Orai1 mRNA expression in RV tissues from control and MCT- rats (n = 5 for the Control group and 6 for the MCT + DMSO group . (O) Localization of Orai1 expression by

immunofluorescence staining of paraffin-embedded RV sections from control rats and MCT-PH rats. Orai1 staining (red) and nucleus (DAPI in blue). (P) Interstitial fibrosis identified with Sirius red staining in RV compartment (at W3) and quantification of the percentage of fibrosis in RV tissue (n = 5 for the Control group, 6 for the MCT + DMSO group and 3 for the MCT + BTP2 group). (Q) Immunofluorescence images of RV sections stained with FITC-conjugated wheat germ agglutinin (WGA, 50 µg/mL, green). Scale bar, 25 µm. Quantification of cardiomyocytes cross-section area (CSA, n = 30 cardiomyocytes measurement per rat from 4 rats for the Control group, 6 for the MCT + DMSO group and 3 for the MCT + BTP2 group). Statistical tests and exact P values are provided in Table S5.

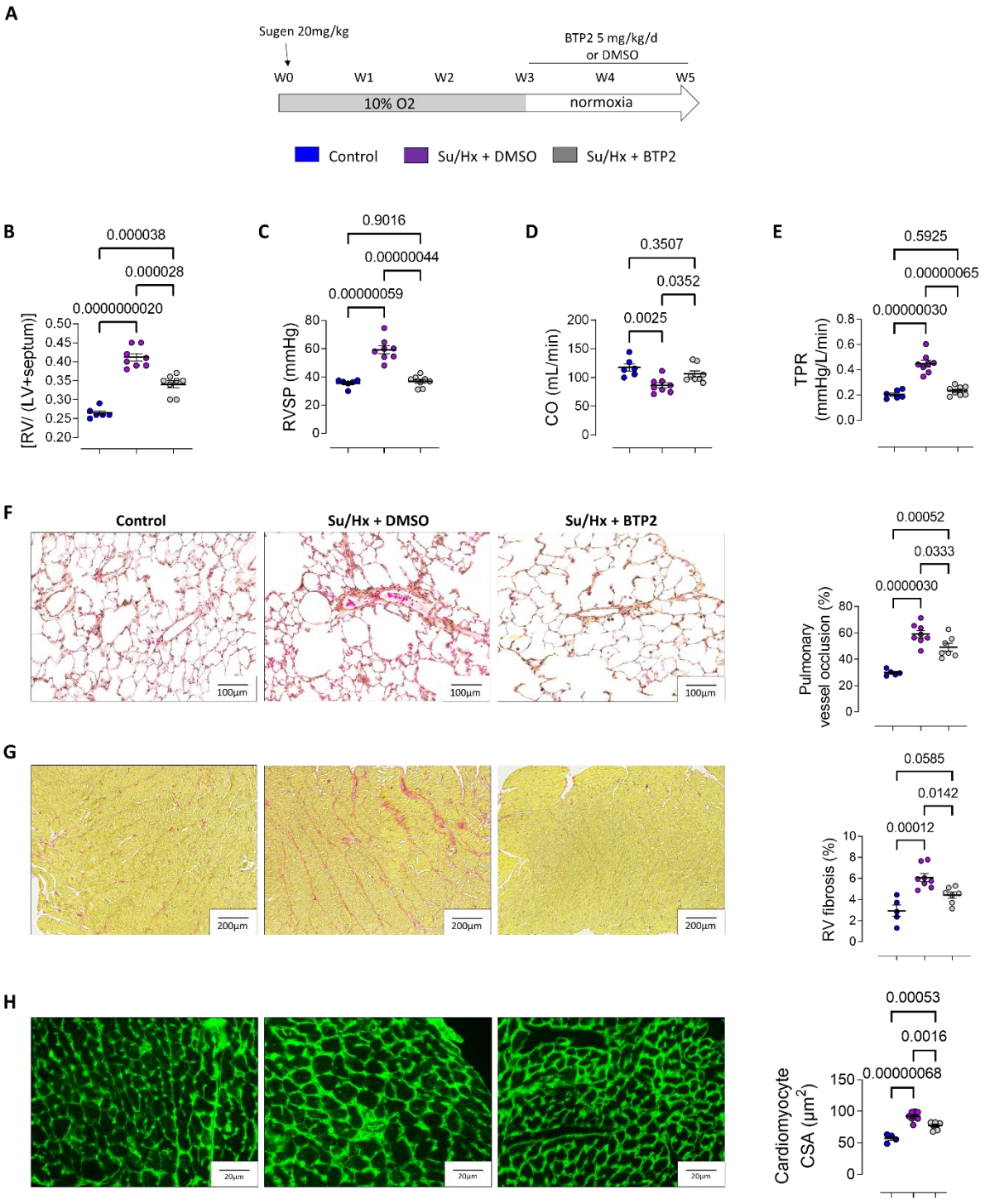

Figure 8

Figure 8: In-vivo pharmacological inhibition of Orai1 with BTP2 reduces the development of Su/Hx-induced PH at pulmonary and RV levels. (A) *In-vivo* experimental design. Rats were maintained in Sugen/hypoxia (Su/Hx) for 3 weeks following 2 additional weeks in normoxic

condition, and BTP2 (5 mg/kg/day) or DMSO was administered between week 3 (W3) and week 5 (W5) by intraperitoneal injection. (B) Fulton's index (n = 6 for the Control group, 8 for the Su/Hx + DMSO group and 8 for the Su/Hx + BTP2 group). (C) RVSP in mmHg (n = 6 for the Control group, 8 for the Su/Hx + DMSO group and 8 for the Su/Hx + BTP2 group). (D) CO in mL/min (n = 6 for the Control group, 8 for the Su/Hx + DMSO group and 8 for the Su/Hx + BTP2 group). (E) TPR (n = 6 for the Control group, 8 for the Su/Hx + DMSO group and 8 for the Su/Hx + BTP2 group). (F) Hematoxylin/eosin/Safran staining of paraffin-embedded lung sections from the control, Su/Hx + DMSO, and Su/Hx + BTP2 groups, and percentage of pulmonary vessel occlusion (%) (n = 5 for the Control group, 8 for the Su/Hx + DMSO group and 7 for the Su/Hx + BTP2 group). (G) Sirius red staining of paraffin-embedded RV sections from the control, Su/Hx + DMSO, and Su/Hx + BTP2 groups and percentage of RV fibrosis (n = 5 for the Control group, 8 for the Su/Hx + DMSO group and 7 for the Su/Hx + BTP2 group). (H) Immunofluorescence images of RV sections stained with FITC-conjugated wheat germ agglutinin (WGA, 50 µg/mL, green). Scale bar, 25 µm. Quantification of cardiomyocytes cross-section area (CSA, n = 30 cardiomyocytes measurement per rat from 4 rats for the Control group, 8 for the Su/Hx + DMSO group and 7 for the Su/Hx + BTP2 group). Statistical tests and exact P values are provided in Table S5.